


Please cite the Published Version

Hubau, Wannes, De Mil, Tom, Van den Bulcke, Jan, Phillips, Oliver L, Angoboy Ilondea, Bhély, Van Acker, Joris, Sullivan, Martin JP , Nsenga, Laurent, Toirambe, Benjamin, Couralet, Camille, Banin, Lindsay F, Begne, Serge K, Baker, Timothy R, Bourland, Nils, Chezeaux, Eric, Clark, Connie J, Collins, Murray, Comiskey, James A, Cuni-Sanchez, Aida, Deklerck, Victor, Dierickx, Sofie, Doucet, Jean-Louis, Ewango, Corneille EN, Feldpausch, Ted R, Gilpin, Martin, Gonmadje, Christelle, Hall, Jefferson S, Harris, David J, Hardy, Olivier J, Kamdem, Marie-Noel D, Kasongo Yakusu, Emmanuel, Lopez-Gonzalez, Gabriela, Makana, Jean-Remy, Malhi, Yadvinder, Mbayu, Faustin M, Moore, Sam, Mukinzi, Jacques, Pickavance, Georgia, Poulsen, John R, Reitsma, Jan, Rousseau, Mélissa, Sonké, Bonaventure, Sunderland, Terry, Taedoumg, Hermann, Talbot, Joey, Tshibamba Mukendi, John, Umunay, Peter M, Vleminckx, Jason, White, Lee JT, Zemagho, Lise, Lewis, Simon L and Beeckman, Hans (2019) The persistence of carbon in the African forest understory. *Nat Plants*, 5 (2). pp. 133-140.

DOI: <https://doi.org/10.1038/s41477-018-0316-5>

Version: Accepted Version

Downloaded from: <https://e-space.mmu.ac.uk/624016/>

Usage rights:  In Copyright

Additional Information: This article was originally published [following peer-review] in *Nature Plants*, published by and copyright Nature.

Enquiries:

If you have questions about this document, contact openresearch@mmu.ac.uk. Please include the URL of the record in e-space. If you believe that your, or a third party's rights have been compromised through this document please see our Take Down policy (available from <https://www.mmu.ac.uk/library/using-the-library/policies-and-guidelines>)

1 **Title**

2 **The persistence of carbon in the African forest understory**

3

4 **Authors**

5 Wannès Hubau ^{1,2,3}*, Tom De Mil ^{1,2}*, Jan Van den Bulcke ^{2,4}, Oliver L. Phillips ³, Bhély Angoboy Ilondea
6 ^{1,5,6}, Joris Van Acker ^{2,4}, Martin J. P. Sullivan ³, Laurent Nsenga ¹, Benjamin Toirambe ¹, Camille Couralet ¹,
7 Lindsay F. Banin ⁷, Serge K. Begne ^{8,3}, Timothy R. Baker ³, Nils Bourland ^{1,9,10,11}, Eric Chezeaux ¹², Connie
8 J. Clark ¹³, Murray Collins ¹⁴, James A. Comiskey ^{15,16}, Aida Cuni-Sanchez ^{17,18}, Victor Deklerck ^{2,4}, Sofie
9 Dierickx ¹, Jean-Louis Doucet ¹⁰, Corneille E. N. Ewango ^{19,20,21}, Ted R. Feldpausch ²², Martin Gilpin ³,
10 Christelle Gonmadje ²³, Jefferson S. Hall ²⁴, David J. Harris ²⁵, Olivier J. Hardy ²⁶, Marie-Noel D. Kamdem
11 ^{8,27}, Emmanuel Kasongo Yakusu ^{1,21,2}, Gabriela Lopez-Gonzalez ³, Jean-Remy Makana ¹⁹, Yadvinder Malhi
12 ²⁸, Faustin M. Mbayu ²¹, Sam Moore ²⁸, Jacques Mukinzi ^{19,29}, Georgia Pickavance ³, John R. Poulsen ¹³, Jan
13 Reitsma ³⁰, Méliissa Rousseau ^{1,11}, Bonaventure Sonké ⁸, Terry Sunderland ^{9,31}, Hermann Taedoumg ⁸, Joey
14 Talbot ³, John Tshibamba Mukendi ^{1,21,32}, Peter M. Umunay ³³, Jason Vleminckx ^{26,34}, Lee J. T. White ^{35,36,37},
15 Lise Zemagho ⁸, Simon L. Lewis ^{3,17}, Hans Beeckman ¹

16

17 * These authors contributed equally to this work.

18

19 **Contact information**

20 whubau@gmail.com, wannes.hubau@africamuseum.be, tom.demil@ugent.be

21 Service of Wood Biology, Royal Museum for Central Africa

22 Tervuren, Belgium, Leuvensesteenweg 13, 3080 Tervuren

23

24 **Affiliations**

25 1 Service of Wood Biology, Royal Museum for Central Africa, Tervuren, Belgium

26 2 UGent-Woodlab, Laboratory of Wood Technology, Department of Environment, Ghent University,

27 Ghent, Belgium

- 28 3 School of Geography, University of Leeds, Leeds, UK
- 29 4 Centre for X-ray Tomography (UGCT), Ghent University, Ghent, Belgium
- 30 5 Institut National pour l'Etude et la Recherche Agronomique, Kinshasa I, Democratic Republic of
31 Congo
- 32 6 Ecole Régionale Postuniversitaire d'Aménagement et de Gestion intégrés des Forêts et Territoires
33 tropicaux (ERAIFT), Kinshasa, Democratic Republic of Congo
- 34 7 Centre for Ecology and Hydrology, Penicuik, UK
- 35 8 Plant Systematic and Ecology Laboratory, Higher Teachers' Training College, University of
36 Yaounde I, Cameroon
- 37 9 CIFOR, Bogor, Indonesia
- 38 10 Forest Resources Management, Gembloux Agro-Bio Tech, University of Liege, Belgium
- 39 11 Resources and Synergies Development, Singapore, Singapore
- 40 12 Rougier-Gabon, Libreville, Gabon
- 41 13 Nicholas School of the Environment, Duke University, Durham, NC, USA
- 42 14 Grantham Research Institute on Climate Change and the Environment, London, UK
- 43 15 Inventory & Monitoring Program, National Park Service, Fredericksburg, VA, USA
- 44 16 Smithsonian Institution, Washington, DC, USA
- 45 17 Department of Geography, University College London, London, UK
- 46 18 Department of Geography and Environment, University of York, York, UK
- 47 19 Wildlife Conservation Society-DR Congo, Kinshasa I, Democratic Republic of Congo
- 48 20 Centre de Formation et de Recherche en Conservation Forestiere (CEFRECOF), Epulu, Democratic
49 Republic of Congo
- 50 21 Faculté de Gestion de Ressources Naturelles Renouvelables, Université de Kisangani, Kisangani,
51 Democratic Republic of Congo
- 52 22 Geography, College of Life and Environmental Sciences, University of Exeter, Exeter, UK
- 53 23 National Herbarium, Yaounde, Cameroon
- 54 24 ForestGEO, Smithsonian Tropical Research Institute, Panamá, Republic of Panama
- 55 25 Royal Botanic Garden Edinburgh, Edinburgh, UK

56 26 Service d'Évolution Biologique et écologie, Faculté des Sciences, Université Libre de Bruxelles,
57 Brussels, Belgium

58 27 Faculty of Science, Department of Botany and Plant Physiology, University of Buea, Buea,
59 Cameroon

60 28 Environmental Change Institute, School of Geography and the Environment, University of Oxford,
61 Oxford, UK

62 29 Salonga National Park, Kinshasa I, DR Congo

63 30 Bureau Waardenburg, The Netherlands

64 31 Faculty of Forestry, University of British Columbia, Vancouver, Canada

65 32 Faculté des Sciences Appliquées, Université de Mbuji-Mayi, Mbuji-Mayi, Democratic Republic of
66 Congo

67 33 Yale School of Forestry & Environmental Studies, New Haven, CT, USA

68 34 Department of Biological Sciences, Florida International University, FL, USA

69 35 Agence Nationale des Parcs Nationaux, Libreville, Gabon

70 36 Institut de Recherche en Ecologie Tropicale, Libreville, Gabon

71 37 School of Natural Sciences, University of Stirling, Stirling, UK

72

73

74

75

76

77

78

79

80

81

82

83 **Quantifying carbon dynamics in forests is critical for understanding their role in long-term climate**
84 **regulation^{1,2,3,4}. Yet little is known about tree longevity in tropical forests^{3,5,6,7,8}, a factor that is vital for**
85 **estimating carbon persistence^{3,4}. Here we calculate mean carbon age (the period that carbon is fixed in**
86 **trees⁷) in different strata of African tropical forests using (i) growth-ring records with a unique**
87 **timestamp accurately demarcating 66 years of growth in one site and (ii) measurements of diameter**
88 **increments from the African Tropical Rainforest Observation Network (23 sites). We find that in spite**
89 **of their much smaller size, in understory trees mean carbon age (74 years) is greater than in sub-**
90 **canopy (54 years) and canopy (57 years) trees, and similar to carbon age in emergent trees (66 years).**
91 **The remarkable carbon longevity in the understory results from slow and aperiodic growth as an**
92 **adaptation to limited resource availability^{9,10,11}. Our analysis also reveals that while the understory**
93 **represents a small share (11%) of the carbon stock^{12,13}, it contributes disproportionately to the forest**
94 **carbon sink (20%). We conclude that accounting for the diversity of carbon age and carbon**
95 **sequestration among different forest strata is critical for effective conservation management^{14,15,16}, and**
96 **for accurate modelling of carbon cycling⁴.**

97
98 Investing in carbon storage and sequestration represent important climate change mitigation strategies³.
99 Forests have a potential to provide both long-lived carbon stocks^{7,17} and long-term carbon sinks^{1,2}. To
100 successfully conserve forest carbon stock and increase forest carbon uptake, we must conserve carbon-rich
101 forests and extend the forested land area³, but decision makers and managers also need to understand the
102 long-term behaviour of carbon within forests^{1,2,3}. Critical questions are: (i) how long does the carbon persist,
103 and (ii) where does it stay longest in the system? Carbon residence time is a direct function of tree
104 longevity^{3,7,17}, but attempts to estimate tree age in tropical rainforests are relatively scarce and often highly
105 contested^{5,6,7,8}. Estimating the ages of the oldest trees in tropical forest stands is particularly subject to debate.
106 While some authors claim that broadleaved trees in the tropics may reach ages of 1000 years or older^{8,18},
107 others estimate maximum ages of not more than 600 years^{5,6}. Furthermore, the oldest carbon in the system is
108 often assumed to be located in large trees⁸. Canopy and emergent trees contain a large proportion of the
109 stand-level biomass^{12,14} but large trees alone may not represent well the entire forest in terms of growth rates,
110 tree lifespan and carbon persistence⁷. Canopy species grow faster¹⁹, but there is a general trade-off between

111 growth and lifespan in organisms^{9,20}. Therefore, long-term carbon storage and sequestration in tropical
112 rainforests may substantially depend on smaller trees too.

113

114 Here, we take advantage of a remarkable rediscovery of a historic forest inventory plot to probe the age
115 structure of African rainforests in a way that has not been possible to date. The Nkulapark plot was
116 established in 1948 in the southwest of the Democratic Republic of the Congo (Supplementary Fig.1). A
117 total of 6315 trees with diameter on breast height (DBH) ≥ 5 cm were tagged and DBH was measured
118 annually for 9 years. In 2014, we rediscovered and measured 450 surviving tagged trees, of which 55 were
119 selected to measure growth ring series. We used the grown-in iron nail as a 1948 timestamp, giving accurate
120 estimates of the DBH growth rate (in mm yr^{-1}) and the rate of growth-ring formation (number of rings per
121 year) over a 66 year period for each tree (Fig.1, Supplementary Table 1). The age of each individual tree (in
122 years) was calculated as the total number of rings from pith to bark, divided by the rate of growth-ring
123 formation (number of rings per year) (Fig.1, Fig.2). We used the five-class Crown Illumination Index of
124 Dawkins & Field (hereafter CII)^{21,22} to compare growth patterns and tree age among the different rainforest
125 strata: understory (CII=1), sub-canopy (CII=2,3), canopy (CII=4) and emergent stratum (CII=5). Understory
126 trees receive no direct light, sub-canopy trees receive lateral light, canopy and emergent trees receive vertical
127 light (Fig.3a).Supplementary analyses show that the rediscovered Nkulapark tree dataset is adequate to
128 compare age differences between forest strata (Supplementary Fig.2, Supplementary Fig.3, Supplementary
129 Discussion).

130

131 We find that the age of the 55 Nkulapark trees with growth-ring series ranges between 129 and 452 years
132 (Fig.2, Supplementary Table 1). There is no clear linear relationship between tree age and their DBH
133 ($p=0.082$, Fig.2a). Understory trees (CII=1) do not differ significantly in age from canopy and emergent trees
134 (CII=4 or 5) ($p=0.254$, boxplot at the right of Fig.2b), while trees in sub-canopy classes (CII=2 or 3) are
135 slightly younger than trees in both the understory and the canopy. Despite their small size, understory trees
136 (CII=1) can be surprisingly old. One *Microdesmis puberula* (TreeID=3545) has an estimated age of 329
137 years, with a DBH of just 156 mm (Supplementary Table 1).

138

139 To test if our findings hold true in a wider geographic context, we compared growth and age patterns among
140 the different forest strata in 23 Central African permanent forest inventory plots¹ (Fig.3, Table 1,
141 Supplementary Fig.1 and Supplementary Table 2). Selected plots had a similar species composition as the
142 Nkulapark. Plots are demarcated rectangles or squares of median size 1 ha where each tree is mapped, tagged
143 and measured according to standard protocols^{1,2}. DBH of each tree with DBH \geq 10 cm was measured at
144 least twice. Small trees that grew larger than 10cm during the monitoring period were recorded as recruits.
145 Trees that died were recorded. We used repeated diameter measurements to estimate the growth rate of each
146 individual tree. We estimated tree age by dividing the final diameter (mm) by the growth rate (mm yr⁻¹),
147 assuming a constant growth rate over the lifetime of a tree⁷. We evaluated the robustness of this age
148 estimation method using the rediscovered Nkulapark trees as a reference (Supplementary Fig.4).
149 Uncertainties are due to relatively short plot monitoring periods (average 9 years), yielding negative or zero
150 growth rates for 9.7% of the trees. To avoid unrealistic tree age estimates, we replaced slow growth rates by
151 a ‘minimum allowed growth rate’, defined as the xth percentile of the growth rate distribution within each CII
152 class. Sensitivity analysis showed that x=25 returned a realistic tree age distribution for our dataset
153 (Supplementary Table 3, Supplementary Discussion). Further analysis suggests that x may be lower if
154 monitoring periods are longer. Finally, we estimated tree-level mean carbon age as the average age of each
155 year ring, weighted by the carbon content of the ring⁷, with a year ring sequence deduced from the growth
156 rate.

157

158 The mean tree age for the 23 plots across the Congo Basin ranged between 131 and 284 years, with an
159 overall mean of 229 years (95% bootstrapped confidence intervals: 212-244 years) (Table 1). Mean tree age
160 in the understory (CII=1) is estimated to be 262 years, which is significantly older than the overall mean
161 (p<0.001) and older than the mean age of the sub-canopy (CII=3, 187 years, p<0.001), the canopy (CII=4,
162 194 years, p<0.001) and emergent classes (CII=5, 221 years, p=0.021) (Table 1). Furthermore, mean carbon
163 age at the tree level is 65 years (95% CI: 61-70). Carbon stored in the understory trees (CII=1) is estimated to
164 be on average 74 years (69-79), which is significantly older than the overall mean (p<0.001) and older than
165 carbon stored in the sub-canopy (CII=3, 54 years, p<0.001) and the canopy (CII=4, 57 years, p=0.001).

166 However, the difference between mean carbon age in the understory (CII=1) versus the emergent class
167 (CII=5, 66 years) is not significant ($p=0.086$) (Fig.3b and Table 1).

168

169 For each forest stratum within each plot, we calculated above-ground biomass-carbon stock (AGC-stock, in
170 Mg C ha^{-1}) and the AGC-sink ($\text{Mg C ha}^{-1} \text{ yr}^{-1}$) using standard methods^{1,2} (Table 1). The AGC-stock
171 represents the carbon reservoir in the system while the AGC-sink represents the net change, calculated as
172 AGC-productivity (additions to the system from tree growth) minus AGC-mortality (losses)¹⁷. The mean
173 AGC-stock in the understory (CII=1) is 19 Mg C ha^{-1} , which is 11% of the total plot-level AGC-stock (Table
174 1). The mean AGC-sink in the understory (CII=1) is $0.21 \text{ Mg C ha}^{-1} \text{ yr}^{-1}$ (Fig.3c), which represents 21% of
175 the plot-level AGC-sink. In contrast, the sub-canopy classes (CII=2 and 3) together contribute about 24% to
176 the AGC-stock, but nothing to the AGC-sink ($-0.01 \text{ Mg C ha}^{-1} \text{ yr}^{-1}$). The understory thus contributes
177 disproportionately to carbon sequestration, considering its relatively small share in the stock, and compared to
178 the limited contribution of the sub-canopy classes.

179

180 **Discussion**

181

182 Results from both the Nkulapark dataset (Fig.2) and the 23 inventory plots (Fig.3, Table 1) show that
183 understory (CII=1) and emergent (CII=5) trees are on average older than sub-canopy trees (CII=3). This
184 pattern can be explained by differences in species composition¹⁵. Understory ‘specialist species’ maintain
185 low growth rates for long periods, resulting in relatively small DBH at older age. Their adaptations allow
186 them to survive in the understory without the need to invest in rapid growth. The sub-canopy classes (CII=2
187 and 3) are populated with suppressed ‘canopy specialists’ that survived a recruitment stage but didn’t reach
188 the canopy yet. These trees are relatively young (Fig.3) and they experience limited light conditions,
189 resulting in mortality rates equaling productivity rates (Table 1). Canopy and emergent trees (CII= 4 and 5
190 respectively) are canopy specialists that have been able to grow rapidly for long periods²³. This is in line with
191 ref.¹⁹ who show that growth rates in emergent trees are high and increase continuously. To test the
192 assumption that high tree and carbon age in the understory may be due to a difference in species
193 composition, we classified species as (i) understory specialists, (ii) non-specialists and (iii) canopy specialists

194 (Supplementary Discussion). This confirmed that understory specialists are on average smaller ($p < 0.001$) but
195 older ($p = 0.003$) than canopy specialists (Supplementary Table 4).

196

197 Furthermore, the Nkulapark dataset shows that there is a significant negative relationship between tree age
198 and growth-ring formation rate (Fig.2b). 91% of the trees in the dataset did not form a growth-ring every
199 year, suggesting an aperiodic growth pattern (shifts of growth to dormancy and back do not occur annually).
200 This aperiodic growth pattern is more prominent in understory trees, which formed fewer growth rings (0.36
201 rings per year) than canopy and emergent trees (0.61 rings per year) ($p = 0.01$; boxplots at the top of Fig.2b).
202 Aperiodic growth patterns translate into significantly slower long-term growth rates: understory trees ($CII = 1$)
203 have a mean DBH growth rate of 1.52 mm yr^{-1} versus 4.99 mm yr^{-1} in emergent trees ($p < 0.001$) (Table 1).
204 The observed differences in growth periodicity (Fig.2b), growth rates (Table 1) and age patterns (Fig.3)
205 among the different forest strata are most likely a result of differences in survival mechanisms which are a
206 function of resource availability^{11,24,25} (Supplementary Discussion).

207

208 Our data show that growth and age distribution of tropical trees in mixed lowland rainforests is complex.
209 Large canopy trees are among the oldest in the rainforest, as suggested by several authors⁸, but as they
210 obtained their size and position by maintaining fast growth rates¹⁹, they are not significantly older than slow-
211 growing small understory specialists (Fig.2, Fig.3, Table 1). Furthermore, while large canopy trees represent
212 the largest share of the carbon stock^{12,13,14}, they suffer most during drought periods²⁶. In comparison,
213 understory trees represent a smaller carbon capital but they are less vulnerable to drought and contribute
214 disproportionately to carbon sequestration. As such, the understory provides long-term stability in forest
215 carbon cycling. Furthermore, the understory is more diverse than the canopy in terms of species
216 composition^{14,15,16}. Therefore, we recommend quantifying forest ecosystem services by considering forests as
217 a whole, with all forest strata providing specific services¹⁶. This is important in Central Africa, where the
218 demand for fuelwood and charcoal could severely affect the understory if only large trees were to be
219 protected^{14,27}.

220

221 Finally, our results suggest that care is required with large-scale modelling of forest carbon accumulation
222 potential and responses to different climate change scenarios⁴. There are two hypothesised responses to
223 increasing atmospheric CO₂ concentrations, possibly explaining the long-term observed AGC-sink in tropical
224 forests^{1,2}: (i) big trees increase their asymmetric competition benefit to the detriment of the rest of the stand,
225 or (ii) suppressed trees do best, as they are closer to their light compensation point^{17,28}. Our results show that
226 both scenarios occur in forest stands, with the understory (CII=1), the canopy (CII=4) and the emergent
227 (CII=5) classes contributing to carbon sequestration, while the sub-canopy classes (CII=2 and 3) do not
228 contribute. Forest and carbon cycle models will need to account for the diversity of carbon age and carbon
229 sequestration potential among the different forest strata. Recent studies have found that forest structure can
230 be predicted from the characteristics of canopy trees^{13,14}, but our results suggest that temporal dynamics
231 differ between forest strata. The long-term persistence of function depends on smaller trees too, which
232 compared to their stature contribute disproportionately heavily to long-term carbon storage, sequestration,
233 and climate resilience.

234

235 **References**

- 236 1. Lewis, S. L. *et al.* Increasing carbon storage in intact African tropical forests. *Nature* **457**, 1003–1006
237 (2009).
- 238 2. Brienen, R. J. W. *et al.* Long-term decline of the Amazon carbon sink. *Nature* **519**, 344–348 (2015).
- 239 3. Körner, C. A matter of tree longevity. *Science* **355**, 130–131 (2017).
- 240 4. Galbraith, D. *et al.* Residence times of woody biomass in tropical forests. *Plant Ecol. Divers.* **6**, 139–
241 157 (2013).
- 242 5. Brienen, R. J. W., Schöngart, J. & Zuidema, P. A. Tree Rings in the Tropics : Insights into the
243 Ecology and Climate Sensitivity of Tropical trees. in *Tropical Tree Physiology* (eds. Goldstein, G. &
244 Santiago, L. S.) **6**, (2016).
- 245 6. Worbes, M. One hundred years of tree-ring research in the tropics – a brief history and an outlook to
246 future challenges. *Dendrochronologia* **20**, 217–231 (2002).
- 247 7. Vieira, S. *et al.* Slow growth rates of Amazonian trees: Consequences for carbon cycling. *Proc. Natl.*
248 *Acad. Sci.* **102**, 18502–18507 (2005).

- 249 8. Chambers, J. Q., Higuchi, N. & Schimel, J. P. Ancient trees in amazonia. *Nature* **391**, 135–136
250 (1998).
- 251 9. Bigler, C. Trade-Offs between growth rate, tree size and lifespan of mountain pine (*Pinus Montana*)
252 in the swiss national park. *PLoS One* **11**, 1–18 (2016).
- 253 10. Kleczewski, N. M., Herms, D. A. & Bonello, P. Effects of soil type, fertilization and drought on
254 carbon allocation to root growth and partitioning between secondary metabolism and ectomycorrhizae
255 of *Betula papyrifera*. *Tree Physiol.* **30**, 807–817 (2010).
- 256 11. Sass-Klaassen, U. Tree physiology: Tracking tree carbon gain. *Nat. Plants* **1**, 15175 (2015).
- 257 12. Bastin, J.-F. *et al.* Seeing Central African forests through their largest trees. *Sci. Rep.* **5**, 1–8 (2015).
- 258 13. Bastin, J.-F. *et al.* Pan-tropical prediction of forest structure from the largest trees. *Glob. Ecol.*
259 *Biogeogr.* **in press**, (2018).
- 260 14. Lutz, J. A. *et al.* Global importance of large-diameter trees. *Glob. Ecol. Biogeogr.* **27**, 849–864
261 (2018).
- 262 15. Memiaghe, H. R., Lutz, J. A., Korte, L., Alonso, A. & Kenfack, D. Ecological Importance of Small-
263 Diameter Trees to the Structure, Diversity and Biomass of a Tropical Evergreen Forest at Rabi,
264 Gabon. *PLoS One* **11**, 1–15 (2016).
- 265 16. Burton, J. I., Ares, A., Olson, D. H. & Puettmann, K. J. Management trade-off between aboveground
266 carbon storage and understory plant species richness in temperate forests. *Ecol. Appl.* **23**, 1297–1310
267 (2013).
- 268 17. Lloyd, J. & Farquhar, G. D. The CO₂ dependence of photosynthesis, plant growth responses to
269 elevated atmospheric CO₂ concentrations and their interaction with soil nutrient status . I . General
270 principles and forest ecosystems. *Funct. Ecol.* **10**, 4–32 (1996).
- 271 18. Laurance, W. F. *et al.* Inferred longevity of Amazonian rainforest trees based on a long-term
272 demographic study. *For. Ecol. Manage.* **190**, 131–143 (2004).
- 273 19. Stephenson, N. L. *et al.* Rate of tree carbon accumulation increases continuously with tree size.
274 *Nature* **507**, 90–93 (2014).
- 275 20. Wright, S. J. *et al.* Functional traits and the growth — mortality trade-off in tropical trees. *Ecology*
276 **91**, 3664–3674 (2013).

- 277 21. Synnott, T. J. *A manual of permanent plot procedures for tropical rainforests. Tropical forestry*
278 *papers* **14**, (1979).
- 279 22. Dawkins, H. C. & Field, D. R. B. *A long-term surveillance system for British woodland vegetation.*
280 *Oxford Forestry Institute Occasional Papers* **1**, (1978).
- 281 23. Hall, J. S., Harris, D. J., Medjibe, V. P. & Ashton, M. S. The effects of selective logging on forest
282 structure and tree species composition in a Central African forest: Implications for management of
283 conservation areas. *For. Ecol. Manag.* **183**, 249–264 (2003).
- 284 24. Couralet, C., Van den Bulcke, J., Ngoma, L. M., Van Acker, J. & Beeckman, H. Phenology in
285 functional groups of Central African trees. *J. Trop. For. Sci.* **25**, 361–374 (2013).
- 286 25. Vico, G., Dralle, D., Feng, X., Thompson, S. & Manzoni, S. How competitive is drought
287 deciduousness in tropical forests? A combined eco-hydrological and eco-evolutionary approach.
288 *Environ. Res. Lett.* **12**, 65006 (2017).
- 289 26. Bennett, A. C., McDowell, N. G., Allen, C. D. & Anderson-Teixeira, K. J. Larger trees suffer most
290 during drought in forests worldwide. *Nat. Plants* **1**, 15139 (2015).
- 291 27. FAO. *The charcoal transition : greening the charcoal value chain to mitigate climate change and*
292 *improve local livelihoods.* (Food and Agriculture Organization of the United Nations, 2017).
- 293 28. Lewis, S. L., Malhi, Y. & Phillips, O. L. Fingerprinting the impacts of global change on tropical
294 forests. *Philos. Trans. R. Soc. B Biol. Sci.* **359**, 437–462 (2004).
- 295 29. Hietz, P. A simple program to measure and analyse tree rings using Excel, R and SigmaScan.
296 *Dendrochronologia* **29**, 245–250 (2011).
- 297 30. Benjamini, Y. & Hochberg, Y. Controlling the False Discovery Rate: A Practical and Powerful
298 Approach to Multiple Testing. *J. R. Stat. Soc. Ser. B* **57**, 289–300 (1995).

299

300 **Correspondence**

301 Correspondence and requests for materials should be addressed to W.H. (whubau@gmail.com).

302

303

304

305 **Acknowledgments**

306 W.H. and T.D.M. were both funded by the Brain program of the Belgian Federal Government
307 (BR/132/A1/AFRIFORD and BR/143/A3/HERBAXYLAREDD). The PhD project of T.D.M and the tenure
308 track of J.V.d.B. were supported by Ghent University Special Research Fund (BOF). Fieldwork was
309 sponsored by the King Leopold III fund for nature exploration and conservation. B.A.I. is supported by the
310 *Institut National pour l'Etude et la Recherche Agronomiques en R.D.Congo* (INERA- RDC- Luki) and the
311 *Ecole Régionale Postuniversitaire d'Aménagement et de Gestion intégrés des Forêts et Territoires tropicaux*
312 (ERAIFT Kinshasa). We thank WWF-RDC (Geert Lejeune), INERA and ERAIFT for facilitating fieldwork
313 in the Luki Reserve. We thank the INERA employees (Jean-Baptiste Ndunga, Jean-Maron, Fils Mbungu
314 Phaka, Leonard Ngoma, Noble, Plaside), the WWF ecoguards and the students of the Universities of
315 Kinshasa (UNIKIN) and Boma for assistance in the field. For assistance with datasets we thank Marlène De
316 Groot, Kévin Lievens, Piet Dekeyser, Stijn Willen and José Kempnaers. This paper is also a product of the
317 AfriTRON network, for which we are indebted to hundreds of institutions, field assistants and local
318 communities. This network has been supported by the European Research Council (291585, "T-FORCES"-
319 Tropical Forests in the Changing Earth System, Advanced Grant to O.L.P.), the Gordon and Betty Moore
320 Foundation, the David and Lucile Packard Foundation, the European Union's Seventh Framework
321 Programme (283080, 'GEOCARBON'), and Natural Environment Research Council (NERC) Consortium
322 Grant 'TROBIT' (NE/D005590/1), 'BIO-RED' (NE/N012542/1) and a NERC New Investigators Grant, the
323 Royal Society, the Centre for International Forestry (CIFOR) and Gabon's National Parks Agency (ANPN).
324 We are indebted to the University of Yaounde I, the National Herbarium of Yaounde, Rougier-Gabon, the
325 Marien Ngouabi University of Brazzaville, WCS-Congo, Salonga National Park, WCS-D.R.Congo, and the
326 University of Kisangani for logistical support in Africa.

327

328 **Author contributions**

329 W.H., T.D.M., J.V.d.B., J.V.A. and H.B. conceived and designed the study. T.D.M. and B.A.I. coordinated
330 collection of Nkulapark data and wood cores. T.D.M. and J.V.d.B. measured growth ring series. W.H.
331 carried out the data analysis and wrote the paper. S.L.L., O.L.P., T.R.B. and Y.M. conceived the AfriTRON

332 forest census network programmes and the Forestplots.net database, and most co-authors helped collecting
333 AfriTRON forest census data. S.L.L., B.S., S.B., A.C.S., W.H., T.S. and L.W.W. coordinated forest plots
334 data collection. M.J.P.S., G.L.G., S.L.L., O.L.P., T.R.B. and G.P. contributed tools to analyze and curate
335 data. All co-authors commented on or approved the manuscript.

336

337 **Competing financial interests**

338 The authors declare no competing financial interests.

339

340 **Figure legends**

341

342 **Figure 1 Example of a wood core (*Greenwayodendron suaveolens*, TreeID=765) showing the 1948 nail**
343 **trace.** The image at the top shows the full core. White lines indicate growth-ring boundaries, numbers
344 indicate growth-rings (counted from bark to pith), black arrows indicate important years. The bark to the
345 right of the figure indicates the year of sampling (2014). The dark discoloration in growth-rings 26 to 35 was
346 caused by oxidates from the iron nail that were transported up and down in damaged vessels and fibers. The
347 right border of the discoloration accurately marks the start of the year 1948. There are 25 rings between the
348 bark and the 1948 nail trace, suggesting that this individual needed on average 2.6 years to form a ring.
349 Using this rate for the 53 rings that were formed before 1948, we find that the first ring in the core was
350 probably formed around 1811. The location of the pith is indicated by the black lines to the left, which
351 follow the direction of the wood rays²⁹. This shows that the distance from the pith to the first ring boundary
352 in the core is about 11 mm. When using the average ring width of rings 78 to 68, we estimate that 7 rings are
353 missing. As such, this individual would be about 224 years old. The three close-ups at the bottom illustrate
354 wood anatomical details used to identify growth-ring boundaries (indicated by white triangles). Ring
355 boundaries in this species are demarcated by distended wood rays and flattening of the fibers. Black scale
356 bars cover 0.2 mm.

357

358 **Figure 2 Variation in tree age inferred from growth-ring patterns in 55 trees where nail traces**
359 **accurately mark the year 1948.** Panel (a) shows the relation between tree age and DBH. Panel (b) shows
360 the relation between tree age and the growth-ring formation rate (number of rings per year) between 1948-
361 2014. In both panels, p-values of simple linear regression models are given in red. Brown dots represent
362 understory individuals (Crown Illumination Index =1), grey dots represent sub-canopy individuals (CII=2
363 and 3), blue dots represent canopy and emergent trees (CII=4 and 5). Boxplots show the first quartile, the
364 median value and the third quartile of the tree age distribution (vertical axis, boxplots to the right) and of the
365 variables in the x-axis (horizontal boxplots at the top of the panels). P-values under boxplots resulted from
366 two-sided Wilcoxon rank-sum tests. Outliers are marked with open circles.

367

368 **Figure 3 Estimation of mean carbon age and AGC-sink per crown illumination category, for 23**
369 **permanent inventory plots in Central Africa.** The 450 rediscovered Nkulapark trees were treated as an
370 additional plot to estimate distributions of mean carbon age. Panel (a) illustrates the Crown Illumination
371 Index (CII) developed by Dawkins and Field (ref.²²), with yellow arrows indicating reception of sunlight
372 (drawing modified from ref.²¹). Understory trees (brown, CII=1) receive no direct sunlight, sub-canopy trees
373 (grey) receive lateral (CII=2) or restricted vertical (CII=3) light, canopy trees (blue, CII=4) are almost
374 completely exposed to vertical light and emergent trees (blue, CII=5) have a crown that is completely
375 exposed to vertical and lateral light. Boxplots in panels (b) and (c) show the distribution of plot-level mean
376 carbon age and plot-level AGC-sink per CII class. Boxplots represent the 25 % quartile, the median value
377 and the 75 % quartile of the plot-level average ages. Outliers are marked with open circles. Comparison
378 among CII classes was performed with Dunn's rank-sum test using the Benjamini-Hochberg adjustment for
379 multiple comparisons³⁰. The grey dotted line shows the overall (plot-level) average age.

380

381

382

383

384

385

metric	All trees	CII 1	CII 2	CII 3	CII 4	CII5	p-value
Tree age (yr)	229 (212-244)	262 (243-282)	210 (196-223)	187 (170-204)	194 (175-212)	221 (192-250)	0.021
Mean carbon age (yr)	65 (61-70)	74 (69-79)	60 (55-64)	54 (49-59)	57 (51-63)	66 (57-75)	0.086
AGC-prod (MgC ha ⁻¹ yr ⁻¹)	3.1 (2.83-3.41)	0.47 (0.4-0.56)	0.53 (0.42-0.67)	0.35 (0.27-0.43)	0.9 (0.69-1.15)	0.82 (0.63-1)	0.015
AGC-mort (MgC ha ⁻¹ yr ⁻¹)	2.05 (1.66-2.48)	0.26 (0.19-0.36)	0.62 (0.49-0.76)	0.28 (0.18-0.38)	0.61 (0.41-0.85)	0.27 (0.07-0.61)	0.058
AGC-sink (MgC ha ⁻¹ yr ⁻¹)	1.05 (0.63-1.5)	0.21 (0.09-0.33)	-0.08 (-0.23-0.05)	0.07 (-0.06-0.2)	0.3 (0-0.59)	0.55 (0.26-0.79)	0.011
AGC-stock (Mg C ha ⁻¹)	177 (159-198)	19 (15-23)	26 (21-31)	17 (12-22)	58 (42-74)	59 (46-75)	<0.001
stem density (stems ha ⁻¹)	428 (392-465)	194 (165-228)	112 (94-130)	38 (33-44)	59 (46-70)	25 (19-31)	<0.001
DBH (mm)	313 (291-338)	161 (154-168)	235 (222-250)	299 (273-326)	435 (397-469)	700 (644-760)	<0.001
DBH growth (mm yr ⁻¹)	2.38 (2.17-2.63)	1.51 (1.35-1.69)	2.16 (1.96-2.38)	2.98 (2.69-3.31)	4.03 (3.71-4.34)	4.99 (4.32-5.68)	<0.001
wood density (g cm ⁻³)	0.59 (0.56-0.61)	0.64 (0.62-0.65)	0.61 (0.6-0.63)	0.59 (0.56-0.61)	0.59 (0.56-0.61)	0.57 (0.53-0.61)	0.006
ratio evergreen:deciduous	3.27 (2.85-3.71)	4.72 (3.86-5.59)	4.61 (2.76-7.85)	3.62 (2.78-4.6)	3.03 (2.09-4.22)	1.78 (0.88-3.43)	<0.001
proportion evergreen trees (%)	55 (52-57)	56 (52-59)	55 (51-59)	56 (52-61)	51 (46-56)	44 (37-52)	0.01
proportion deciduous trees (%)	18 (16-20)	14 (12-17)	19 (16-22)	21 (17-25)	26 (21-31)	35 (28-41)	<0.001

389 **Table 1 Estimation of plot-level mean tree age, mean carbon age, aboveground carbon sink (AGC-**
390 **sink), AGC-stock and leaf habit per crown illumination category, for 23 permanent forest plots.** The
391 450 rediscovered Nkulapark trees were treated as an additional plot for estimation of tree age and mean
392 carbon age (first two rows). All metrics were averaged per plot and per CII class. Mean values are given in
393 bold, 95% confidence intervals are given between brackets. Components of the AGC-sink are AGC-
394 productivity and AGC-mortality. Components of AGC-stock are diameter (DBH), wood density and stem
395 density. Comparison among CII classes was performed with Dunn's rank-sum test using the Benjamini-
396 Hochberg adjustment for multiple comparisons³⁰; the reported p-values compare CII1 and CII5.

404 **Online Methods**

405

406 *Site description.* The Nkulapark is a phenology and tree-growth monitoring plot covering 174 ha within the
407 Luki Man and Biosphere reserve, located in the southern Mayumbe mountains in the Democratic Republic of
408 the Congo²⁴ (Supplementary Fig.1). The region experiences a humid tropical climate with a dry season
409 between mid-May and mid-October and a short dry season from mid-December to mid-February. Yearly
410 precipitation ranges from 649 mm to 1853 mm with a mean precipitation of 1173 mm. Temperature ranges
411 between 19 °C and 30 °C with a mean temperature of 25.5 °C²⁴. The Nkulapark is situated almost entirely in
412 a catchment with a valley and a ridge and includes several microclimatic conditions. The semi-deciduous
413 lowland forest consists of (i) mature forest dominated by *Prioria balsamifera*, (ii) old regenerating forest
414 dominated by *Terminalia superba*, (iii) mixed-species mature forest and (iv) modified forest patches^{31,32}.

415

416 *Nkulapark plot design in 1948.* The Nkulapark was established and managed by *the Institut National pour*
417 *l'Etude Agronomique du Congo Belge* (INEAC), which was later renamed *Institut National pour l'Etude et*
418 *la Recherche Agronomique en R.D.Congo* (INERA, <http://www.inera-drc.org>). The person in charge of the
419 tagging and the measurements was Léon Toussaint, who worked as a botanist in the Luki reserve between
420 1946 and 1952³³. The planning of the plot was first announced in the INEAC-Luki annual report of 1946³⁴. A
421 total of 29.2 km of observation paths were cut in the forest in 1947, following the contour lines of the Nkula
422 river valley (Supplementary Fig.1)³¹. A total number of 6315 trees were tagged by the end of 1947³¹, so we
423 assume that first wood formation after tagging occurred during the wet season that started in October 1948.
424 Tree selection was performed by randomly selecting trees from the pool of trees > 5 cm DBH in 1948. The
425 Nkulapark area was mapped, showing the locations of the largest tagged trees. From 1948 to 1957 yearly
426 diameter measurements were performed on all tagged trees³⁵. Mortality events were recorded in the
427 datasheets. Trees were measured at a height of 1.3 m and the point of measurement (POM) was indicated on
428 the tree with a horizontal line of lead-based paint. For trees with buttresses or deformities, the POM was
429 raised to a point high enough to avoid the irregularities interfering with diameter measurements at
430 subsequent censuses. For trees with extremely high buttresses, diameters were estimated. For the same 6315
431 trees, weekly phenology observations were recorded. Phenological observations were done for leaf habit,

432 flowering, fruiting and seed dissemination. The plot was abandoned in 1957 but the datasheets were kept in
433 the library of the INERA station in Luki and digitized in 2008²⁴ and 2014.

434

435 *Rediscovering Nkulapark trees in 2014.* Each of the original 6315 Nkulapark trees were labelled during the
436 first census in 1948 with a zinc number tag that was attached to the tree using an iron nail of 8 cm long. A
437 part of these trees were indicated on the original 1948 map. During a first prospective field campaign in
438 august 2014, this map was digitized and georeferenced with QGIS (QGIS development team, 2016) using
439 landmarks such as easily rediscovered trees, contour lines and observation paths that were still visible and
440 could be tracked with a Garmin 64s GPSmap (see Supplementary Fig.1). Based on this map, we pinpointed
441 the approximate location of 1521 individuals that were recorded as alive during the last census in 1957.
442 During a second field campaign in September- October 2014, these 1521 individuals were searched for. 450
443 of them were found alive, 16 were found dead and the remaining 1057 could not be relocated and were
444 assumed to be dead and rotten away, albeit some may have been missed (see Supplementary Fig.2,
445 Supplementary Fig.3, Supplementary Discussion for an in-depth analysis of survivorship rates). The original
446 1948 tree tags and nails of the rediscovered trees were either still present outside the trunk or detected inside
447 the tree using a metal detector (BHJS, Bounty Hunter, USA). Scars on the trunk indicated the presence of an
448 overgrown nail, and repelled number tags were sometimes found on or in the ground nearby the tree using
449 the metal detector. In most cases, the numbers on the tags were still readable. On 95% of the rediscovered
450 trees, the lead-based paint of the POM was still visible, allowing a representative DBH measurement.
451 Comparison of DBH, DBH growth rates and tree age distribution in the original dataset of Nkulapark trees
452 versus the dataset of rediscovered trees, showed that the rediscovered dataset is slightly biased towards
453 discovering slower-growing trees, but this bias affected both the classes of understory and canopy ‘specialist’
454 species (Supplementary Fig.3). Hence, the rediscovered tree dataset is representative to compare growth and
455 age patterns among the different forest strata in the Nkulapark area.

456

457 *Sampling Nkulapark trees in 2014.* Wood samples for growth-ring analysis were taken from rediscovered
458 trees if following criteria were met : (a) the nail was still present in the wood, either totally grown-in or
459 partly sticking out of the trunk, (b) the exact position of the nail could be identified visually or with the metal

460 detector, (c) the nail was not overgrown by excessive wound tissue, buttresses or other deformities. As such,
461 increment cores or stem discs were taken near the nail for 58 of the rediscovered trees. For each sampled
462 tree, increment cores were taken a few centimetres above, below, to the left and to the right of the nail using
463 a 40cm Pressler bore. For each tree, two additional cores were taken at 120° from the nail trace along the
464 circumference of the tree. As such, 6 increment cores were available for each tree. This maximised the
465 chance of sampling the pith of the tree. To study and describe the reaction of the wood after tagging,
466 additional larger wood samples containing the nail were extracted from 30 trees using a saw and a chisel.

467

468 *Visualizing and measuring growth-ring series.* For each wood core, growth-ring series were visualized using
469 two imaging methods as described by ref.³⁶: (i) first, density profiles were calculated from X-ray CT scans of
470 entire wood cores, then (ii) the cores were surfaced with a core microtome³⁷ and scanned using a flatbed
471 scanner (EPSON Perfection 4990 PHOTO). To obtain X-ray CT volumes, cores were scanned at 110 µm
472 resolution with the Nanowood CT facility from the Centre for X-ray Computed Tomography of Ghent
473 University (UGCT, www.ugct.ugent.be)³⁸, developed in collaboration with XRE (www.xre.be; now part of
474 the TESCAN ORSAY HOLDING a.s.). Reconstruction was performed with the Octopus software package
475 on a GeForce GPX 770 4GB GPU^{38,39}. X-ray and flatbed scans were analysed using the toolchain for tree-
476 ring analysis described by De Mil et al. (ref.³⁶). This toolchain semi-automatically indicates the growth-ring
477 boundaries and calculates growth-ring width series. Depending on the visibility of the growth-ring patterns,
478 either the X-ray or the flatbed scans were used to check growth-ring boundaries and measure growth-ring
479 widths. Growth-ring boundaries were distinguished using visual wood anatomical characteristics such as
480 distended rays, flattened fibers and terminal parenchyma bands^{5,40,41}. For unclear ring boundaries,
481 microscopic thin sections were taken to study wood anatomy at high resolution using an Olympus BX60
482 microscope (Fig.1).

483

484 *Detecting the 1948 nail trace.* Discolorations or wound tissue formed as a reaction on the tagging were
485 visible in the cores taken near the nail. The surface of these stem discs was sanded to a few millimetres
486 above the nail and the anatomy was observed using an Olympus BX60 microscope. The nails were
487 remarkably well preserved inside the trees, probably due to cathodic protection of the iron by the zinc of the

488 tags. Hence, discolorations or wound tissue were visible in each of these samples. Discolorations were
489 recognizable as darkened tissue in otherwise light-coloured wood (Fig.1). Discolorations occurred in cells
490 that were formed before the nail was inserted, due to oxidation processes between the wood and the iron nail.
491 Water in vessels and fibers in the neighbourhood of the nail (especially those damaged by the nail) spread
492 these oxidates upwards and downwards. Therefore, the discolorations in these cells are also detectable on
493 samples that were taken a few centimetres under or above the nails. Vessels and fibers that were formed after
494 the tagging were not damaged, hence did not show discolorations. As such, the boundary of the discoloration
495 accurately serves as a timestamp indicating the year of tagging (1948). Furthermore, wound-induced
496 deformities occurred in the wood that was formed after the nail was inserted. This wound tissue is
497 characterized by increased woody productivity around the nail, forming a lump in the growth-rings that were
498 formed just after the nail was inserted. This lump formation is not present in the wood that was formed
499 before tagging.

500

501 *Estimating tree age using growth rings and nail traces.* Six cores were assessed for each tree. For some trees,
502 none of the cores contained the pith because (i) the tree radius exceeded the borer length or (ii) the pith was
503 eccentric and missed. In these cases, the core with the largest number of visible rings was used to estimate
504 the total number of growth-rings. The missing core length from the end of this core to the pith was estimated
505 using the intersection of three lines of ring boundaries marked along the rays, as described by ref.²⁹ (see
506 Fig.1 for an example). We estimated the number of rings in the missing core part by dividing the missing
507 core length by the average ring width of the 5 oldest rings of the sampled core. We tested the robustness of
508 this method by rerunning the analysis using the average growth rates of the 5, 10, 15 and 20 oldest rings. We
509 found that the overall average tree age and the trends observed in Fig.2 are not sensitive to varying the
510 method used to estimate the number of rings in the missing part of the core. The core with the clearest nail
511 trace was used to count the number of rings formed after the year of tagging (1948). We used the number of
512 growth-rings formed between 1948 (nail mark) and 2014 (cambium) as a reference to calculate the number
513 of years the individual needed to form one ring (years per ring). We then multiplied this ratio with the total
514 number of rings formed before 1948 to estimate the age of the tree (Fig.1 and Fig.2). Three individuals were

515 not used for analysis because the estimated missing core length of each core exceeded 20 cm. As such,
516 growth-ring series of 55 trees were retained (Supplementary Table 1).

517

518 *Permanent forest inventory plots.* To test if our findings hold true in a wider geographic context, we
519 estimated mean tree age and carbon age of the different forest strata in 23 Central African permanent forest
520 plots located in four different Central African countries (Cameroon, Gabon, Congo Brazzaville, D.R.Congo)
521 (Supplementary Fig.1 and Supplementary Table 2). Plots were selected if at least 65% of the trees belonged
522 to species that also occur in the Nkulapark. Furthermore, plots selected for analysis conformed to the
523 following criteria^{1,2,42}: (1) plots had an actual plot area of ≥ 0.2 ha, (2) plots were georeferenced, (3) all trees
524 with $DBH \geq 100$ mm were measured, (4) the majority of stems were identified to species level, (5) plots had
525 at least 2 censuses, (6) plots had a total monitoring length of ≥ 3 years, (7) plots were situated within
526 structurally intact, apparently mature forest (excluding young or open forests), (8) plots were free from major
527 human impacts, (9) plots were located at ≥ 50 m from the anthropogenic forest edge, (10) altitude was below
528 1500 m.a.s.l., (11) mean annual air temperature was $\geq 20.0^{\circ}C$, (12) mean annual precipitation was ≥ 1000 mm
529 yr^{-1} , (13) plots were located in terra firme forest. For analysis purposes, plots smaller than 0.5 ha that were
530 within 1 km of each other and located in similar forest types were merged (i.e. the LME cluster). All selected
531 plots are part of the African Tropical Rainforest Observatory Network (AfriTRON; www.afritron.org). These
532 data are curated in the ForestPlots.net database⁴³, and subject to identical quality control and quality
533 assurance procedures. All calculations of plot data metrics described hereafter were performed using the R
534 statistical platform⁴⁴, version 3.2.1.

535

536 *Estimating AGC-stock.* For each tree and each census, Aboveground Biomass at the tree level (AGB, Mg
537 $stem^{-1}$) was estimated using a published allometric equation for moist forests including terms for diameter
538 (DBH, mm), dry wood density (ρ , $g\ cm^{-3}$) and total tree height (H, m)⁴⁵ :

$$539\ AGB = \frac{0.0673 \times (\rho \times (\frac{DBH}{10})^2 \times H)^{0.976}}{1000} \quad (\text{formula 1}).$$

540 Wood density values were derived from the dryad database (www.datadryad.org). Stems were matched to
541 species-specific wood density values or the mean values for the genus or family, following ref.¹ and⁴³.

542 Heights were calculated using a single height-diameter model (Weibull) for central African lowland terra
543 firme forests published by ref.⁴⁶, using commands implemented in the R-package BiomasaFP⁴⁷.

544 Aboveground Biomass-Carbon (referred to as AGC) is considered as 47% of the AGB following IPCC
545 recommendations⁴⁸. For each individual tree in the plot dataset, AGC-stock was calculated as the mean of the
546 first and last censuses.

547

548 *Estimating AGC-sink.* For the calculation of AGC-sink, only the first and the last censuses were used for
549 each plot. First, AGC- productivity ($\text{Mg C stem}^{-1} \text{ yr}^{-1}$) for each stem surviving the monitoring period, was
550 calculated as the difference between its total AGC at the end census minus the total AGC at the start census
551 of the interval, divided by the census interval length (yr). AGC-productivity for stems recruited during the
552 monitoring period (i.e. reaching $\text{DBH} \geq 100 \text{ mm}$), was calculated in the same way, assuming $\text{DBH} = 0 \text{ mm}$ at
553 the start of the interval. AGC-mortality for each tree that died during the monitoring period ($\text{Mg C tree}^{-1} \text{ yr}^{-1}$)
554 was calculated as the AGC at the start of the monitoring period, divided by the total monitoring length (yr).

555 AGC-productivity at the stand level ($\text{Mg C ha}^{-1} \text{ yr}^{-1}$) was then calculated as the sum of tree-level productivity
556 estimates of all survivors and recruits. AGC-mortality at the stand level ($\text{Mg C ha}^{-1} \text{ yr}^{-1}$) was calculated as the
557 sum of tree-level mortality estimates of all dead trees in the subset. We corrected for unobserved components
558 of biomass growth and mortality due to census interval length effects, as discussed by ref.², ref.⁴⁹ and ref.⁵⁰.

559 A method to correct productivity and mortality rates for these uncertainties was developed by ref.⁴⁹ and
560 applied by ref.². This correction accounts for (i) trees that recruit and die within the same interval (i.e.
561 unobserved recruits) and (ii) growth of trees that grow and die within the interval (i.e. unobserved biomass
562 growth from mortality, which is not recorded because dead trees are not measured). As such, for each census
563 interval, we calculated unobserved recruitment and unobserved mortality components ($\text{Mg ha}^{-1} \text{ yr}^{-1}$) using
564 the formulas proposed by ref.⁴⁹ and both components were added to both the AGC-productivity and AGC-
565 mortality estimates. Estimates of the unobserved biomass components usually accounted for less than 3% of
566 the total AGC-productivity and AGC-mortality. Finally, the AGC-sink was calculated as stand-level AGC-
567 productivity minus AGC-mortality. Commands to calculate AGC-stock and AGC-sink are implemented in
568 the BiomasaFP R package⁴⁷.

569

570 *Tree age inferred from DBH growth rates in permanent inventory plots.* For each tree within the permanent
571 forest inventory plots, we estimated the age by dividing the DBH (mm) in the final census with the DBH
572 growth rate (mm yr⁻¹) of the tree itself. For each tree, we averaged the DBH growth rate over all census
573 intervals preceding the last census. This method uses the actual growth rate of each tree, which is accurate
574 for healthy trees but returns unrealistic age estimates for trees with (i) slightly negative growth rates, (ii) zero
575 growth rates or (iii) very slow growth rates. Such slow growth rates may be recorded in all DBH classes.
576 First, slow growth rates in large DBH classes may occur when a tree is diseased or at the end of its life
577 (senescence). These growth rates may not be representative for the total lifespan of these trees. Secondly,
578 small growth rates may be recorded for small suppressed trees if their growth is so slow that it cannot be
579 recorded with sufficient precision using standard census procedures. Hence, these growth rates are replaced
580 by growth rates that are comparably small but yield a realistic tree age estimate. As such, we chose a
581 ‘minimum allowed growth rate’ per CII class, following ref.⁷. We calculated the minimum allowed growth
582 rate for each CII class as the 25th percentile (=first quartile) of the growth rate distribution within the CII
583 class. For each tree with a growth rate slower than the minimum allowed rate, we replaced the growth rate by
584 the minimum allowed growth rate of the CII class. We conducted a sensitivity analysis to check how results
585 vary when varying the minimum allowed growth rate: we reran the analysis using the 10th, 15th, 20th, 25th and
586 30th percentile of the growth rate distribution within each CII class as a minimum allowed growth rate
587 (Supplementary Discussion and Supplementary Table 3). We used the average tree age in the dataset of 450
588 rediscovered Nkulapark trees as a reference to evaluate the tree-age estimation method based on DBH
589 growth rates (Supplementary Figure 4).

590

591 *Mean carbon age.* As a tree grows, it increasingly stores more carbon. Carbon near the bark of the tree is
592 younger than carbon in the pith. As such, mean carbon age of a tree does not equal total tree age. We
593 calculated mean tree-level carbon age using the same formula as ref.⁷:

594
$$\text{mean carbon age} = \frac{\sum_{i=1}^n (C_i \times A_i)}{\sum_{i=1}^n (C_i)} \quad (\text{formula 2}),$$

595 with:

596 C_i = carbon content of the i^{th} ring (kg),

597 A_i = age of the i^{th} ring (yr),

598 n = nr of rings.

599

600 The carbon content of the i^{th} ring is calculated as the carbon content of a tree with the DBH of ring i minus
601 the carbon content of a tree with the DBH of ring $i-1$. To estimate carbon age in trees without measured
602 growth-ring series (permanent inventory plots), we used the final DBH and the DBH growth rate (in mm yr⁻¹)
603 to deduce a year-ring pattern, assuming that the growth rate was constant over the lifetime of the tree.

604

605 *Classification of tree species and statistical analysis.* We used the Nkulapark phenology data published by
606 ref.²⁴ to classify tree species as evergreen or deciduous. To distinguish between understory, sub-canopy,
607 canopy and emergent trees in the Nkulapark and the permanent forest plots, we used the Crown Illumination
608 Index (CII) of Dawkins & Field (ref.²²). Fig.3 illustrates the 5 classes with a drawing modified from ref.²¹.
609 The Crown Illumination Index was recorded in 23 of the selected permanent inventory plots. In each plot
610 where the index was recorded, each tree was attributed to one of the CII classes. The index was attributed in
611 the field, mostly during one census and mostly by a single person. We estimated mean tree age, mean carbon
612 age, mean AGC-stock and mean AGC-sink for each of the CII classes in each plot where the index was
613 recorded. None of the metrics reported in Table 1 meet the criterion of homogeneity of variances (Bartlett
614 test). Therefore, differences among the CII classes were tested using the non-parametric Dunn's rank-sum
615 test. To avoid the multiple comparison problem, we used the Benjamini-Hochberg p-value adjustment³⁰
616 ('dunn.test' package in R⁴⁴).

617

618 *Data availability.* The input data and R-scripts to generate the figures and tables are available for download
619 using the following private link : <https://figshare.com/s/06c793575d3b52ef5574>. Images of wood cores are
620 available using the following link : <https://figshare.com/s/e6101fe7d330f8ea140a> . This folder also contains
621 all annotation documents needed to visualize growth ring boundaries on the wood samples (please consult
622 the README document for guidelines). Wood samples used to conduct this analysis are stored in the
623 Tervuren xylarium
624 (<http://www.africamuseum.be/collections/browsecollections/naturalsciences/earth/xylarium>). These samples

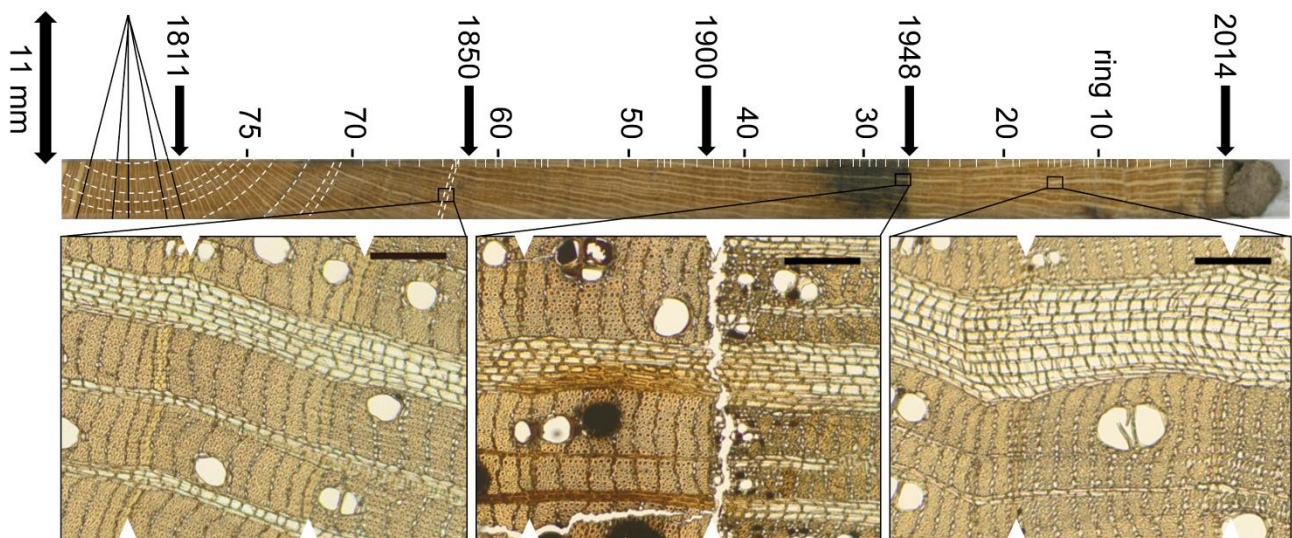
625 may be studied, within the Tervuren xylarium, upon request addressed to the curator H.B.
626 (hans.beeckman@africanmuseum.be) or the corresponding author W.H. (whubau@gmail.com).

627

628 **References (methods only)**

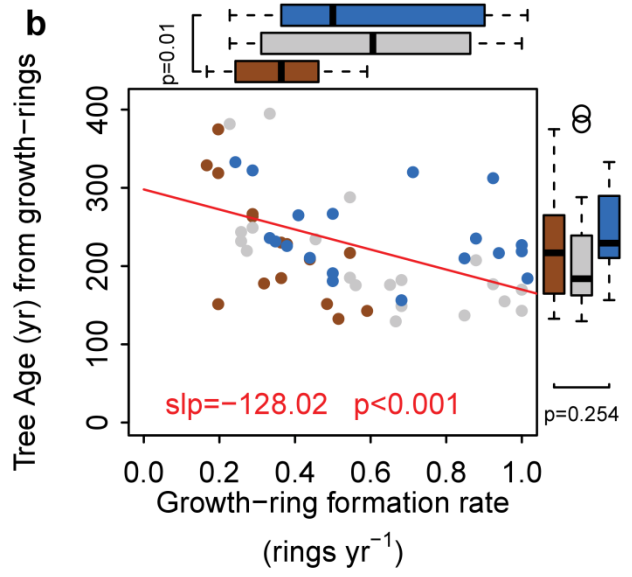
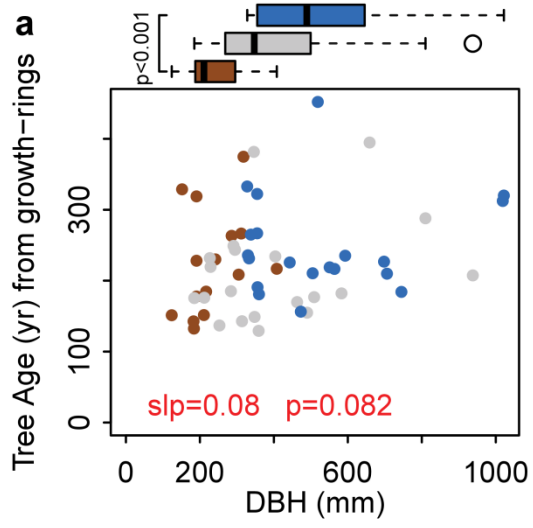
- 629 31. INEAC. *Rapport Annuel INEAC-Luki*. (1947).
- 630 32. Coppieters, G. Inventaris van het archief van de Rijksplantages en de Regie der Plantages van de
631 Kolonie, het Nationaal Instituut voor de Landbouwkunde in Belgisch-Congo en de
632 Documentatiedienst voor Tropische Landbouwkunde en Plattelandsontwikkeling 1901-1999. (2013).
- 633 33. Académie Royale des Sciences d'outre-mer. *Biographie Coloniale Belge/Biographie Belge d'Outre-*
634 *Mer, Tome IX*. (2015).
- 635 34. INEAC. *Rapport Annuel INEAC-Luki*. (1946).
- 636 35. INEAC. *Rapport Annuel INEAC-Luki*. (1948).
- 637 36. De Mil, T., Vannoppen, A., Beeckman, H., Van Acker, J. & Van Den Bulcke, J. A field-to-desktop
638 toolchain for X-ray CT densitometry enables tree ring analysis. *Ann. Bot.* **117**, 1187–1196 (2016).
- 639 37. Gärtner, H. & Nievergelt, D. The core-microtome: A new tool for surface preparation on cores and
640 time series analysis of varying cell parameters. *Dendrochronologia* **28**, 85–92 (2010).
- 641 38. Dierick, M. *et al.* Recent micro-CT scanner developments at UGCT. *Nucl. Instruments Methods*
642 *Phys. Res. Sect. B Beam Interact. with Mater. Atoms* **324**, 35–40 (2014).
- 643 39. Vlassenbroeck, J. *et al.* Software tools for quantification of X-ray microtomography at the UGCT.
644 *Nucl. Instruments Methods Phys. Res. Sect. A Accel. Spectrometers, Detect. Assoc. Equip.* **580**, 442–
645 445 (2007).
- 646 40. Worbes, M. Tree-Ring Analysis. *Encycl. For. Sci.* 586–599 (2004).
- 647 41. Tarelkin, Y. *et al.* Growth-ring distinctness and boundary anatomy variability in tropical trees. *IAWA*
648 *J.* **37**, 275–294 (2016).
- 649 42. Phillips, O. & Baker, T. Field manual for plot establishment and remeasurement - RAINFOR. *Rainfor*
650 *22* (2009). doi:10.13140/RG.2.1.1735.7202
- 651 43. Lopez-Gonzalez, G., Lewis, S. L., Burkitt, M. & Phillips, O. L. ForestPlots.net: A web application
652 and research tool to manage and analyse tropical forest plot data. *J. Veg. Sci.* **22**, 610–613 (2011).

- 653 44. R Development Core Team. R: A language and environment for statistical computing. (2008).
- 654 45. Chave, J. *et al.* Improved allometric models to estimate the aboveground biomass of tropical trees.
655 *Glob. Chang. Biol.* **20**, 3177–3190 (2014).
- 656 46. Feldpausch, T. R. *et al.* Tree height integrated into pantropical forest biomass estimates.
657 *Biogeosciences* **9**, 3381–3403 (2012).
- 658 47. Lopez-Gonzalez, G., Sullivan, M. & Baker, T. BiomasaFP package. Tools for analysing data
659 downloaded from ForestPlots.net. R package version 1.1. Available at
660 <http://www.forestplots.net/en/resources>. (2015).
- 661 48. Aalde, H. *et al.* IPCC Guidelines for National Greenhouse Gas Inventories. Volume 4: Agriculture,
662 Forestry and Other Land Use. Chapter 4: Forest Land. *Forestry* **4**, 1–29 (2006).
- 663 49. Talbot, J. *et al.* Methods to estimate aboveground wood productivity from long-term forest inventory
664 plots. *For. Ecol. Manage.* **320**, 30–38 (2014).
- 665 50. Clark, D. a *et al.* Measuring net primary production in forest concepts and field methods. *Ecol. Appl.*
666 **11**, 356–370 (2001).



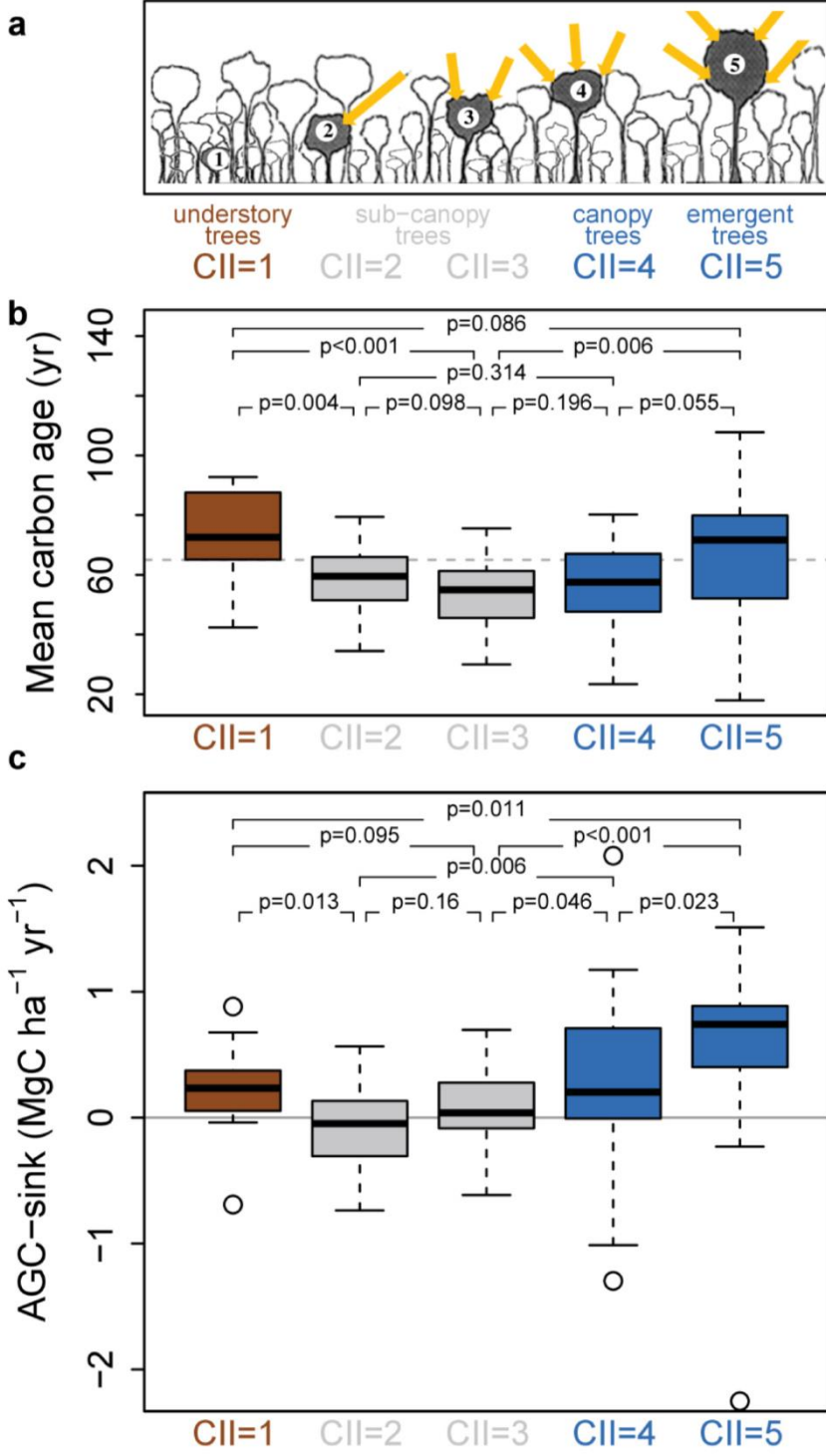
667

668



669

670



671